Rapid-scan pump–probe spectroscopy with high time and wave-number resolution: optical-Kerr-effect measurements of neat liquids

M. J. Feldstein, P. Vöhringer, and N. F. Scherer

Department of Chemistry, The University of Pennsylvania, Philadelphia, Pennsylvania 19104

Received November 17, 1994; revised manuscript received March 24, 1995

A system for the rapid-scan (RS) acquisition of time-resolved nonlinear spectroscopic signals, capable of femtosecond resolution over a range of tens of picoseconds, is presented. Operationally, the system is based on a magnetically driven, commercially available velocity transducer that continuously scans a probe delay line relative to a fixed delay line while data are recorded on the fly and in real time. A simple calibration and data time-scale linearization are carried out and tested on optical-heterodyne-detected optical-Kerr-effect measurements. These results are compared with data acquired with a detection system that is based on a stepped delay-line lock-in amplifier. It is found that the RS system is favorable in several areas of signal acquisition, including signal-to-noise ratio, acquisition time, spectral resolution in the Fourier-transformed data, and immunity to artifacts such as baseline distortions.

1. INTRODUCTION

Femtosecond nonlinear spectroscopies have, in recent years, been implemented in the time-resolved study of vibrational[1–4] and optical[5–9] dephasing and chemical reaction dynamics.[4,10–12] These experimental advances have come about as a result of ever-shorter pulse durations (~6 fs),[13] increasingly stable pulse sources (colliding-pulse mode-locking,[14] Ti:sapphire[15–17]), and enhanced signal detection methods.[18–21] In many cases the chemical process being studied requires measurements on a range of time scales from femtoseconds to picoseconds or longer. One such example is time-dependent fluorescence studies of molecular solvation in which inertial solvent responses occur within 0.5 ps while Debye relaxation can occur even on 100-ps time scales.[22]

Time-resolved optical pump–probe measurements employing high-repetition-rate lasers systems are commonly carried out with a data-acquisition method that is based on a lock-in amplifier (LIA). Signal detection could involve pump beam modulation (i.e., chopping) and point-by-point signal processing through a LIA, which is referenced to the chopper frequency and phase. In this method the optical path length for a probe pulse is stepped relative to a fixed pump pulse path length to measure a pump-induced modulation of the probe beam. The temporal waveform reflecting the material response to excitation is formed in a point-by-point fashion by measurement of the induced modulation at a series of delay times. Whereas this method is clearly effective for many measurements,[1,2,5–7,16,19] including photoacoustic and thermal lens spectroscopies,[23,24] it does have several inherent drawbacks.

The several potential shortcomings of LIA or boxcar (i.e., gated integrator) detection methods include (1) baseband detection and $1/f$ noise, (2) the time required for data acquisition, and (3) modulation of the laser fluence directed toward the sample. First, aside from the details of particular noise sources in lasers (i.e., water cooling, microphonics, thermal fluctuations, plasma oscillations, etc.), noise in experimental measurements tends to scale as $1/f$.[25] The LIA is not totally effective for filtering low-frequency noise even with a small bandpass setting because establishing the transient waveform requires acquisition of many data points. Slow thermal fluctuations and low-frequency drifts of the laser intensity will introduce artifacts into the signal because these drifts may be significant over the several-minute time scale of each measurement. Therefore time consuming repetitive averaging of the waveform must be performed to remove these types of noise.

Second, obtaining a good signal-to-noise ratio (SNR) for each data point requires a reasonably long time constant, τ_{RC}, on the LIA. Furthermore, to ensure that the exponential response of the filter has adequate time to respond to the signal one must wait a delay of $4\tau_{RC}$ before recording each new data point. Thus, for a 100-ms time constant, yielding a 10-Hz bandwidth, 0.4 s is required between measurements of successive data points. Add to this enough time for any vibrations, or ringing, of the scanned mounts to stop, time for recording and averaging multiple samples at a single point, and time to transfer the data to the PC; each delay time step requires approximately 1 s of acquisition time. For a scan of the order of 1000 data points, the total scan time is approximately 20 min. Moreover, to obtain a better SNR from a LIA one must either narrow the bandpass by increasing the time constant or average multiple scans together and, either way, increase the acquisition time.

Third, LIA detection of a pump–probe signal or application in other nonlinear spectroscopies requires chopping the pump pulse while detecting the induced modulation of the probe. Excitation beam chopping can result in periodic heating and cooling in thermally sensitive systems. Unless this thermal response is the goal of the measurement, it could introduce artifacts into the

0740-3224/95/081500-11$06.00

signal. In some cases this may be an even more significant limitation of LIA detection than the inherent long measurement time. For example, thermal fluctuations are especially problematic in measurements in which the optical pump is directed into the tunneling junction of a scanning tunneling microscope.[26] It has been found that the scanning tunneling microscope's tunneling current is significantly coupled to and modulated by heating and expansion of the tunneling tip induced by chopped optical excitation of surface plasmons in the tunneling junction.

One approach to dealing with these shortcomings in the case of high-repetition-rate laser systems is a rapid-scan (RS) experimental configuration to acquire data quickly and with steady-state illumination.[27] The concept behind the RS data-acquisition method is to continuously scan a probe delay line relative to a fixed delay line and record data on the fly and in real time. Arithmetic signal averaging is used to yield a good SNR in the recorded waveform. The concept of a RS is not a new one[28]; however, the method has been employed only for nonlinear spectroscopic measurements in a limited number of experiments.[20,29,30–32] Further, apart from that of Ralph and Grischkowsky,[31] no RS study with four decades of time resolution, i.e., tens of picoseconds with sub-10-fs time-step resolution, has been presented to our knowledge. This may be due in part to the limited commercial availability of RS systems and data-acquisition hardware,[33] especially in comparison with the overabundance of stepper motor scanners and LIA's.

In this paper we present a complete RS experimental system and data-acquisition hardware based on commercially available equipment for pump–probe nonlinear-optical measurements with sub-10-fs time-step resolution over tens of picoseconds. This apparatus is capable of acquiring pump–probe signals faster than the LIA method, with superior SNR, steady-state illumination, and increased spectral resolution (in the Fourier-transformed data) as well as having several other benefits. The RS system and the data-acquisition method are described in Section 2 along with the laser system and the optical arrangement used to perform a series of time-resolved measurements. Signal averaging as well as time-scale calibration and linearization results are given in Section 3. Additionally, to illustrate the effectiveness of the RS method, optical-heterodyne-detected optical-Kerr-effect (OHD-OKE) measurements of several simple liquids taken with this RS apparatus are presented and compared with measurements taken with a LIA data-acquisition method.[34] A discussion of the results, including, some limitations of the RS system and improvements currently being implemented, is given in Section 4. A summary of the method and an overview of future experimental applications are presented in Section 5. Finally, a Jones matrix analysis of the OHD-OKE local oscillator and probe fields is given in Appendix A.

2. EXPERIMENT

A. Laser System and Optical Arrangement

The laser system, the RS delay line, the OHD-OKE experimental scheme, and the signal detection/processing electronics are shown in Fig. 1. The laser system consists of a cw argon-ion laser (Coherent Innova 310) pumping a home-built four-mirror Kerr-lens mode-locked Ti:sapphire laser with an X-fold cavity configuration. Intracavity fused-silica prisms and a short Ti:sapphire crystal (4 mm) allow for routine generation of 25-fs duration pulses. A 10% output coupler enables pulse energies of 6–7 nJ to be obtained at a 76-MHz repetition rate. Extracavity fused-silica prisms allow for compensation of the quadratic residual chirp from the laser and for precompensation for dispersion in the subsequent experimental optics including wave plates, beam splitters, lenses, and sample cell. The pump–probe setup employs a precision hollow corner cube (PLX, <5-mrad deviation in parallelism) attached to the velocity transducer that is used to provide the continuous RS of the optical probe pulse delay relative to the fixed pump pulse delay. An externally mounted linear variable differential transformer (LVDT) monitors the position of the velocity transducer and is used as a scope trigger. Operationally, the weak probe pulse was derived from the Ti:sapphire pulse train by the use of a surface reflection from an uncoated fused-silica substrate; the remainder of the pulse serves as the intense pump beam. The time delay of the probe beam with respect to the pump was controlled by the continuously moving velocity transducer, typically operating at 20 Hz with 3-mm total displacement. The total probe pulse delay, in the configuration used with a retroreflector following the velocity transducer, was proportional to four times the displacement of the corner cube, that is, 40-ps total delay.

The OHD-OKE measurements were performed in a standard Kerr effect geometry.[35] The probe beam was passed through a pair of crossed Glan–Taylor polarizers (Karl Lambrecht) that have an extinction ratio of better than 10^5. The pump, which was polarized 45 deg with respect to the probe, and probe pulses were focused to a common spot in the sample and recollimated afterward. The probe pulse then passed through the analyzer, as noted above, which was oriented 90 deg with respect to the polarizer. The maximum extinction was limited by the static birefringence of the sample cell; this was positioned to minimize both the probe leakage through the analyzer and scattered pump light from reaching the detector. A $\pi/2$ local oscillator field for optical heterodyne detection was derived by a small rotation of a quarter-wave plate located in the probe beam (see Appendix A). To maintain a large signal-to-background ratio and limit

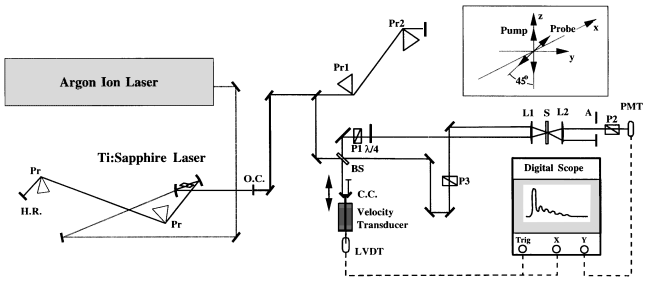

Fig. 1. Schematic of experimental configuration. Home-built Ti:sapphire laser: Pr's, intracavity prisms; H.R., high reflector; O.C., output coupler; Pr1, Pr2, extracavity prisms; BS, beam splitter; C.C., corner cube; P1–P3, Glan-Taylor polarizers; L1, L2, 50-mm achromatic lenses; A, aperture. The inset with arrows indicates the polarization conditions for the OKE measurements.

probe noise, small rotations were used to yield a local oscillator field greater than the signal field but of the same order of magnitude.[27] The time-dependent pump-induced birefringence was measured by detection of the product of the signal and local oscillator fields with a red-enhanced photon detector, i.e., a photomultiplier tube (PMT; Hamamatsu, R928). The PMT output was directed into a digital oscilloscope (Tektronics, TDS-420), which was triggered on the rising edge of the external LVDT signal.

We obtained the transient birefringence response of each simple liquid, including chloroform, acetonitrile, carbon tetrachloride, mesitylene, alkanes, and alcohols, by taking the difference of two scans with local oscillator fields of equal amplitudes but with opposite phases (i.e., $\pm\pi/2$).[4,36] These measurements were analyzed for their linearity, time-scale calibration, SNR, and, through a deconvolved Fourier transformation (see Subsection 3.C below), spectral resolution and peak locations. The RS OHD-OKE results were compared with OHD-OKE measurements taken with the same experimental apparatus but with a stepped delay line and LIA detection in place of the RS velocity transducer and digital oscilloscope. The lock-in amplifier used for these reference experiments was an all-digital dual-phase instrument (Stanford Research, SR830) that has SNR characteristics superior to those of analog versions.[37] A more comprehensive discussion of the home-built Ti:sapphire laser and the OHD-OKE measurement can be found in Ref. 34.

B. Rapid-Scan Apparatus

The RS apparatus is based on a magnetically driven velocity transducer and control unit (Ranger Scientific, VT-900A-X, EC-900) designed for use in Mössbauer spectroscopy. The unit, a schematic of which is seen in Fig. 2, is programmable to provide scan frequencies from 1 to 100 Hz with displacements up to ± 10 mm with a constant-velocity waveform. For the double-pass optical geometry described above this yields time delays of up to 260 ps. In addition to the internally generated waveform, any external waveform, from a function generator, for example, may be supplied to drive the unit. A built-in position sensor provides continuous position measurements that are internally digitized with 10-bit resolution and could provide an independent position reference signal. In addition to the built-in position sensor, a precision LVDT (Lucas-Schaevitz, DC-E125) was added externally to the end of the velocity transducer shaft to provide continuous analog position measurements over ranges up to 6 mm. The analog output of the LVDT can then be digitized with resolution greater than that obtained from the internal position sensor.

Data were acquired on a digital oscilloscope capable of 100 MS/s sampling rates and up to 15-bit vertical resolution, depending on acquisition mode. For single-scan acquisition, data were recorded in the oscilloscope's "Hi Res" mode, where resolution enhancement owing to oversampling yields 15-bit resolution. For a repetitive signal the oscilloscope's averaging mode was used with 8-bit digitizing resolution. The LVDT signal was used both as the scope trigger and as the position data. The position (x) and the signal (y) data were recorded simultaneously. The digital scope was usually set to acquire 5000 data points (although 15,000 or more could be acquired) in a mode where it continuously averaged pump–probe transient waveforms as fast as they were generated, typically 20 Hz. After some period of averaging on the scope, typically 10–500 waveform acquisitions, the data were transferred to a PC where they were stored and averaged together with subsequent waveforms from the digital oscilloscope. Total acquisition time for this process was a function of only the scan rate and the number of scans averaged together. Operating at 20 Hz, the scope could average together more than 5,000 scans of 5,000 data points to yield an excellent SNR in approximately 5 min.

3. RESULTS

A. Signal Averaging and Data Point Spacing

The effect of signal averaging on SNR is demonstrated in Figs. 3(a) and 3(b), which show the measured instrument response function, i.e., autocorrelation, from a single scan and from 1000 averaged scans, respectively. The SNR of the averaged signal is improved more than 15-fold over that from a single scan. This is noteworthy because only 1 min was required to produce the 1000-scan averaged result. Similar improvements in the SNR of OHD-OKE measurements were found with the RS signal acquisition and averaging technique.

Although the LVDT output provided a direct position, and hence an optical time delay, measurement for each signal data point, small accelerations and decelerations of the velocity transducer resulted in these data points' being nonequally spaced in delay time. This is not a problem if one is interested only in the analysis of the time-domain data, as with the measurement of an autocorrelation to determine the system's time resolution, because the LVDT-derived time scale accurately represents the points in an x–y format. However, some signal analysis techniques, such as those based on the fast-Fourier-transform algorithm, require the data points to be equally spaced in time. Figures 4(a) and 4(b) show the raw time–domain OHD-OKE data measured for carbon tetrachloride (CCl_4) and the imaginary part of its deconvoluted Fourier transform, respectively. Sharp features are expected in the Fourier spectra based on Raman spectral data for the 216- and 314-cm^{-1} modes[34,38]; the uncorrected data, however, yield oscillatory patterns. These oscillatory features are artifacts that are indicative of a nonlinear time base with unequal point spacing.

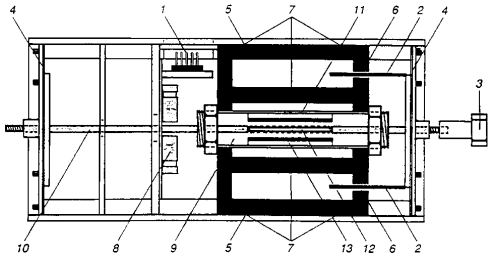

Fig. 2. Schematic of Ranger Scientific VT-900A-X velocity transducer and corner cube: 1, electrical connector; 2, electrodynamic drive coil; 3, corner cube; 4, drive shaft suspension; 5, permanent drive magnets; 6, magnetic ring gaps; 7, magnetic cores; 8, internal power amplifier; 9, custom position sensor mechanism space inside a grounded shield; 10, nonmagnetic composite shaft; 11, grounded shield, for position sensor space; 12, sensor magnet; 13, position sensor coil.

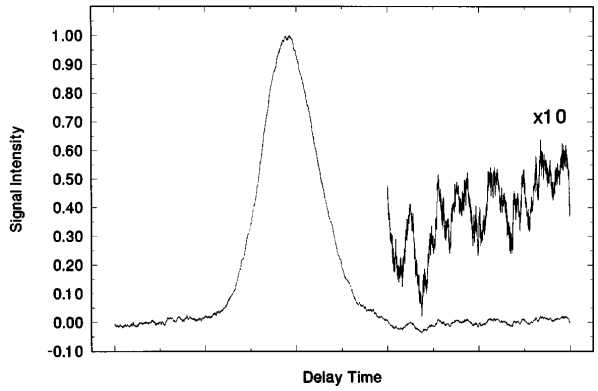

(a)

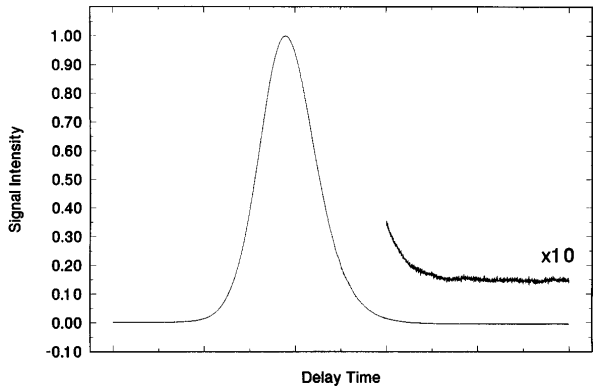

(b)

Fig. 3. Normalized RS autocorrelations. (a) Single scan, (b) 1000 scans averaged in 1 min.

Thus the measured signal requires some processing before it is entirely useful for a more comprehensive analysis. A reliable method, detailed below, was devised to calibrate the time scale and linearize the data point spacing.

B. Calibration and Linearization

The following method was employed to calibrate the time scale of the RS system. First, the instrument response function, or pump–probe autocorrelation, was determined from the optical Kerr response of a 1-mm fused-silica window. This autocorrelation provided a measure of the time response of the Ti:sapphire pump–probe experimental apparatus. Second, a precision stepper motor translation stage (Melles-Griot, Nanomover, 50-nm step resolution) that was part of the fixed delay line was stepped and the peak position (i.e., channel) of an average of 25 RS autocorrelations was recorded while the velocity transducer was scanned at 20 Hz with 3-mm total displacement. The effect of stepping the translation stage was to shift the signal or autocorrelation and its corresponding data channels with an independently known change in delay time. This method yielded accurate delay-time values for each of the scope's data channels that were based on the stepper motor translation stage's position. The calibration was performed so that the entire data-acquisition range of the scope would be scanned over 1000 data points [see Fig. 5(a)]. Although to a first approximation the calibration shows the velocity transducer's motion to be linear, it can be seen that the point-to-point spacing varies by ± 0.2 fs, or $\pm 4\%$ [see Fig. 5(b)]. Consequently, signals taken with this RS method must be corrected to account for the fact that the recorded data points are not equally spaced in time.

This correction is accomplished quite easily by fitting a third-order polynomial to the calibration data and interpolating delay time values for all 5000 data-acquisition channels. A linear time base is also created from the minimum delay time to the maximum delay time in 5000 equally spaced points, step size 4.8 fs. Comparison of the calibration time curve with the linear time base once again shows the nonlinearity of the velocity transducer [see Fig. 5(c)]. A cubic spline was performed on the calibration curve data and the signal; then signal values for each of the 5000 delay-time data points were mapped by interpolation onto the equally spaced points' time axis, which yielded a signal with data points equally spaced in time. Fourier analysis could be carried out on the resulting data without any further correction.

C. RS versus LIA Detection: OHD-OKE Measurements

We tested the quality of the data obtained by the RS system by performing OHD-OKE measurements of several neat liquids, including CCl_4 and 1,3,5 trimethylbenzene (mesitylene). The optical Kerr effect is a transient birefringence, i.e., a polarization-dependent refractive index, induced by an intense optical pulse passing through a material.[21,39] Vibrational frequencies and time scales of vibrational dephasing as well as molecular reorientation

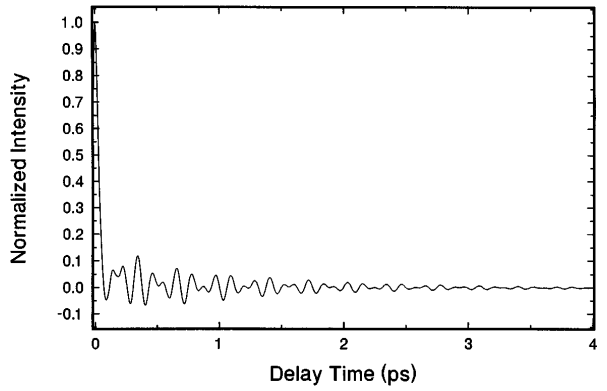

(a)

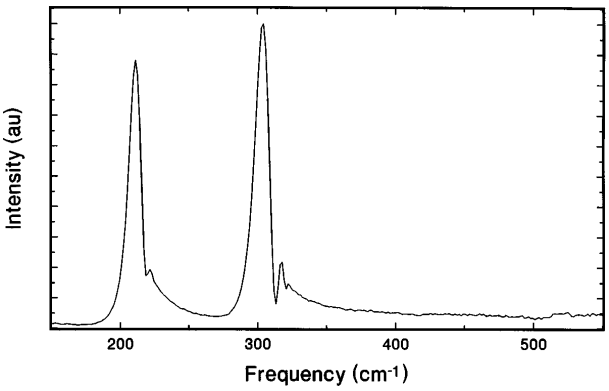

(b)

Fig. 4. Raw CCl_4 OHD-OKE data. (a) Time domain, (b) imaginary deconvolved Fourier spectra.

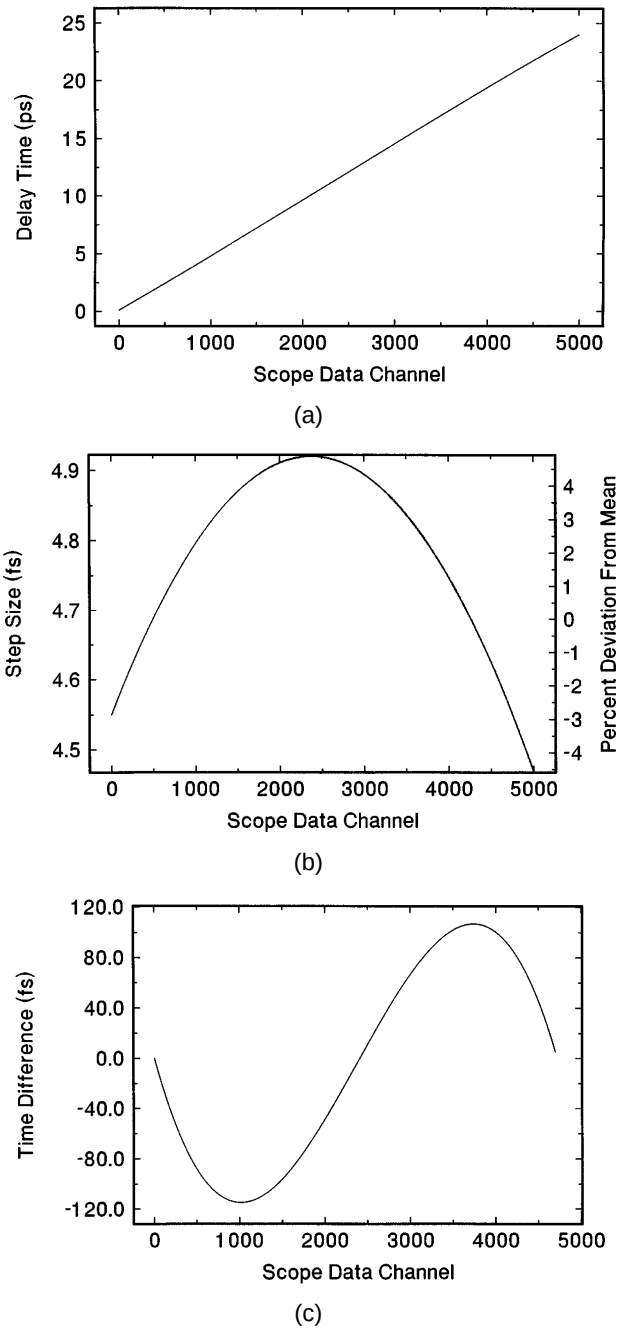

Fig. 5. Time-axis calibration and linearization. (a) Calibration of scope data channel (x) versus Nanomover delay time (y). (b) Point-to-point deviations in step size spacing, scope channels (x) versus time difference (y, left) and percent deviation from mean (y, right). (c) Point-to-point differences between calibration curve and constructed linear time base (y) versus scope data channel (x).

time scales can be determined from OKE measurements, as the signal exhibits sinusoidal modulations with frequencies corresponding to the Raman active modes that are accessible within the bandwidth of the optical excitation pulse. The dynamics, initiated by impulsive excitation by the pump pulse, can be monitored directly by the change of the polarization state of the time-delayed probe pulse. OHD is performed by addition of a local oscillator field of known phase to the signal field and measurement of the product or interference of the two on the detector. This approach serves to linearize the signal detection [i.e., $\chi^{(3)}(t)$ versus $|\chi^{(3)}(t)|^2$] and enhances the SNR by applying a controlled amplitude local oscillator.

A comparison of the OHD-OKE data obtained by RS and by LIA detection is shown in Fig. 6. The time–axis-corrected RS and the LIA OHD-OKE data for CCl_4 are plotted together, showing quite clearly that RS has the better SNR. Quantitatively, the RS SNR is more than an order of magnitude better than the LIA-detected results. This is particularly noteworthy because the very high SNR RS OHD-OKE data were acquired in 5 min. The waveform resulted from 5000 averaged scans taken at a 20-Hz repetition rate with 3-mm displacement (yielding as much as 40-ps total delay time) of which a 25-ps range was recorded. By contrast, the 1000 data points of the LIA measurements, which cover only a 4-ps range, required approximately 20 min to acquire. The two measurements were obtained within 1 h of each other with the same laser system and identical local oscillator levels.

An additional benefit of the longer time scale and the greater number of points in the RS waveform is the increased spectral resolution obtained in the Fourier-transformed CCl_4 data. A comparison of the imaginary parts of the deconvolved Fourier spectra obtained from RS and LIA data is shown in Fig. 7. The deconvolution nec-

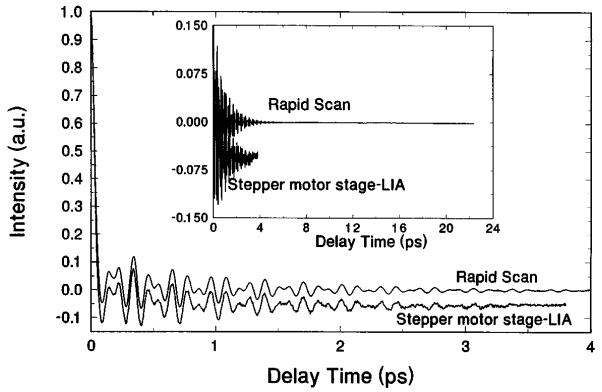

Fig. 6. CCl_4 OHD-OKE time-domain data: linearized RS and stepper motor translation-stage–lock-in-amplifier waveforms. The inset shows the full time-axis data recorded over 24 ps. The stepper motor translation-stage–LIA waveform is offset by −0.05 unit.

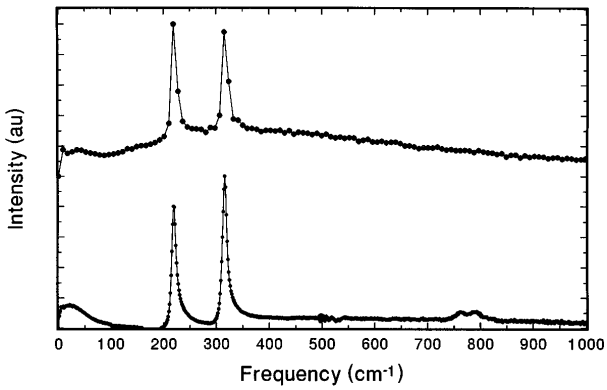

Fig. 7. Imaginary deconvolved Fourier spectra of CCl_4: linearized RS (lower trace) and stepper motor translation-stage–lock-in-amplifier (upper trace with dots) waveforms. Each dot is a single data point.

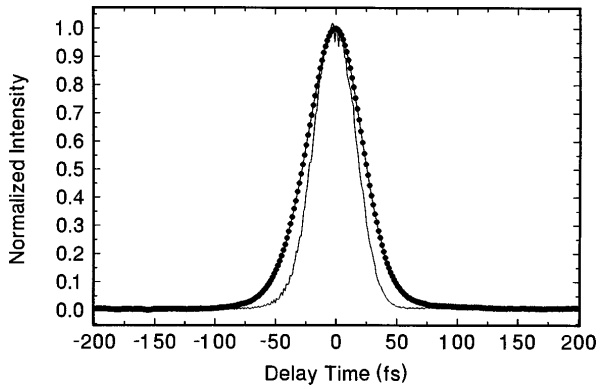

Fig. 8. Normalized autocorrelations: RS, 1000 averaged (connected points), stepper motor translation-stage–lock-in amplifier (solid curve).

essary to account for the finite duration of the laser pulses was carried out as in Ref. 34. Briefly, one removes the instrument response by dividing the Fourier transform of the OHD-OKE time-domain data by the Fourier transform of the pump–probe autocorrelation. The RS autocorrelation used for the deconvolution is shown in Fig. 8 along with the analogous LIA measurement. The spectra again clearly show that RS data acquisition yields a superior SNR. Figure 8 shows that the RS instrument response function is, however, broader than that measured with the LIA. An explanation for the cause of this broadening is discussed below in Subsection 3.D.

The plots of the imaginary parts of the deconvolved Fourier spectra, which are equivalent to the frequency-domain depolarized Raman spectrum,[39] clearly demonstrate the enhanced spectral resolution of the RS data; the RS data points are spaced by 1.5 cm^{-1}, compared with the LIA data points, which are spaced by 9 cm^{-1}. Comparison of the wave-number values of the spectral peaks with the frequencies in the CCl_4 Raman spectrum[38] shows that the RS data are accurate and that the calibrated experimental time scale is reliable. Further, the RS spectrum also establishes that the data points are linearly spaced. This is indicated by the lack of satellite features following each spectral peak. These additional features were present in the raw data shown in Fig. 4(b), indicating that the points were not equally spaced in time. These artifacts are eliminated through proper calibration and linearization of the time axis by the approach described in Subsection 3.B.

Figure 9(a) shows the RS OHD-OKE data for mesitylene. Again, the excellent SNR and the large time range obtainable with the RS apparatus are clearly illustrated in the OHD-OKE time-domain signal. Further, the accuracy of the intramolecular vibrational mode frequencies, the symmetrical shape of the spectral peaks in the imaginary part of the deconvolved Fourier spectrum in Fig. 9(b), and excellent agreement with the cw Raman data[30] demonstrate the correctness of the time-scale calibration. The imaginary part of the deconvolved Fourier spectrum shows a lack of recurrences following each peak, indicating that the OHD-OKE signal has been properly linearized. Most importantly, a comparison of the RS OHD-OKE imaginary Fourier spectrum with one acquired with a LIA system shows that the RS method achieves significant enhancements in resolution. First, the spectral peaks at 228 and 276 cm^{-1} are poorly defined in the LIA data, which have only four or five points for each peak. Further, the correct value of these peaks is not accurately determined because of the low spectral resolution of the LIA method. On the other hand, the RS data have six times the spectral resolution and are able to determine accurately the correct value of these spectral features. A second and even more significant advantage of the RS system compared with the LIA method is its ability to resolve very low-frequency features in the Fourier spectra. This is illustrated clearly in Fig. 9(b) in the region below 20 cm^{-1} where the RS data resolve a sharp feature that is completely missing in the LIA results.

D. Scan-to-Scan Jitter

One limitation of the RS apparatus was an inherent scan-to-scan jitter, which was found to range up to ± 7 channels, or, with 4.8 fs per channel, to ± 34 fs, as determined by the drift of the peak position in the femtosecond transient. A histogram of this jitter is shown in Fig. 10. The consequence of this jitter is that the time resolution of the averaged signal is blurred and becomes less than the resolution of each individual scan when successive scans are continuously averaged on the digital oscilloscope. This effect, i.e., loss of time resolution, is illustrated by a comparison of the autocorrelations shown in Fig. 8. The full width at half-maximum (FWHM) of

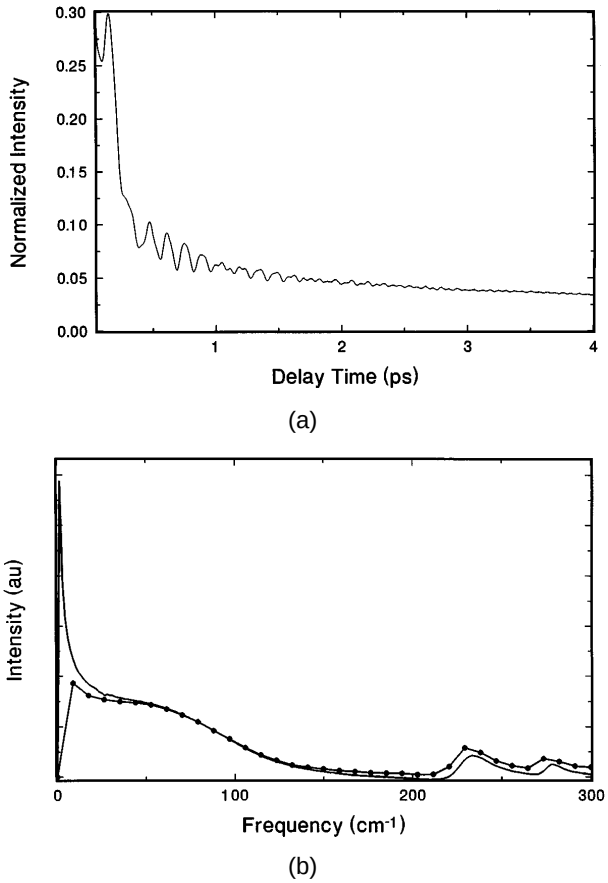

Fig. 9. OHD-OKE data for mesitylene. (a) RS time domain waveform. (b) Imaginary deconvolved Fourier spectra, RS (solid curve), stepper motor translation-stage–lock-in amplifier (connected points).

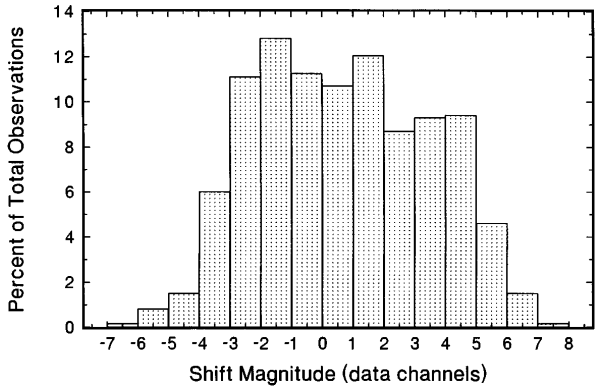

Fig. 10. Histogram of scan-to-scan jitter. Each data channel corresponds to 4.7 fs.

the LIA response function is 42 fs, whereas that of the RS response function is 54 fs. The difference between these two response functions can be attributed to the convolution of the 42-fs FWHM LIA response function with a 34-fs FWHM Gaussian broadening function, which is the measured variance that is due to scan-to-scan jitter. This convolution yields a 54–fs FWHM response function, which corresponds exactly to the RS autocorrelation FWHM.

4. DISCUSSION

A. Signal Averaging

The RS system presented in this paper is an efficient and effective method for the acquisition of pump–probe transients with femtosecond resolution over large time ranges up to 260 ps. As presented in Fig. 3, the ability of the system to improve the SNR of a measurement through continuous high-speed signal averaging by more than an order of magnitude compared with slow stepping methods is quite dramatic. Further, the effectiveness of noise reduction through signal averaging is limited only by the memory capabilities of the digitizer,[40] and one can extend them even further by storing several sets of data and averaging them together at a later time.

B. Calibration and Linearization

The calibration and linearization of the RS system's experimental time scale are carried out through a simple and reliable procedure that accounts for nonlinearities in the velocity transducer's motion. This procedure makes it possible to analyze data more thoroughly and to extract more information than is possible in the time domain alone. The accuracy of the system's calibration and linearization is well demonstrated by the position and shape of the sharp spectral features in the Fourier spectra shown in Figs. 7 and 9(b). The high quality and accuracy of the calibration and linearization in these corrected data are especially evident from a comparison with the Fourier spectra of raw data, shown in Fig. 4(b), which have several satellites after each peak.

This calibration and linearization procedure, which determines the delay time of the RS measurement based on the relative position of the Nanomover stage, can also be carried out with other equipment. For example, a lower-quality and less expensive stepper delay line could certainly be used for this purpose. Alternatively, an air-spaced étalon placed in the pump–beam path could be used to generate a train of equally spaced pulses suitable for the purpose of calibration.

C. RS versus LIA Detection: OHD-OKE Measurements

A comparison of the RS system with other, more common methods of time-resolved optical pump–probe measurements is quite favorable. Specifically, a comparison of OHD-OKE measurements taken with the RS system with those acquired with a lock-in amplifier based system highlights several of the important features, abilities, and potential applications of the RS equipment.

In general, the RS data-acquisition method is preferable to the LIA method because it is less susceptible to artifacts arising from multiple sources. First, the RS data-acquisition method is superior because it provides better immunity to slow thermal fluctuations and low-frequency drifts of the laser intensity. One obtains immunity in RS data acquisition by measuring the entire transient signal at a rate faster than the thermal fluctuations and laser drifts. This is important for reliable signal acquisition because slow drifts, which may be significant over the several-minute time scale of LIA signal acquisition, can introduce artifacts into the data. Second, RS signal acquisition does not require modulation of the laser fluence directed toward the sample and thus can reduce the presence of thermal artifacts in the signal that arise from the periodic heating and cooling of the sample.

One of the most important advantages of the RS compared with LIA system is an improved SNR. With the RS an order-of-magnitude improvement in SNR can be achieved in one fourth of the acquisition time. This is clearly evident in the time-domain signals presented in this paper and is particularly significant for weakly absorbing systems or small amplitude features. Further, these results are consistent with the predictions of Moon for the large-signal limit where pump fluctuations are the dominant noise source.[27] Also, as noted above, the only limit on SNR improvement in RS is the memory capabilities (resolution and depth) of the digitizer.

An additional and significant advantage of the RS data-acquisition and -averaging method is the ability to acquire a waveform over a 40-ps time without sacrificing time-step spacing. This is important for the study of long-lived (picosecond) processes, which have dynamics that occur on a femtosecond time scale. Further, increasing the time range allows for enhanced sensitivity to low-frequency features. Compared with the LIA method, the RS is particularly favorable for analysis of low-frequency responses because signal averaging reduces noise in all frequency ranges whereas a lock-in amplifier, with its inherent baseband detection method, is much less effective at removing low-frequency noise.

As demonstrated by the data shown in Figs. 7 and 9(b), the sixfold enhancement in spectral resolution in the RS is particularly important for analysis of vibrational linewidths and low-frequency features. This enhancement in spectral resolution is directly related to the extended scan range of the RS measurement, whereas the high time resolution and small point spacing are necessary for accurate determination of high-frequency features. In the case of the OHD-OKE measurements

presented here the extended scan range, which yields the spectral enhancement, is necessary because, as shown in Fig. 6, the impulsively induced intramolecular vibrational and orientational motions persist for times longer than a few picoseconds. Furthermore, rotational diffusion responses that decay with time constants of several picoseconds require measurement over three (or more) decades (base e) to establish these decay times accurately. The benefit of longer-time measurement while high time resolution and small data point time spacing are maintained is clearly seen in the Fourier-transform data in Fig. 9(b) for mesitylene. The RS data make possible accurate characterization of the solvent susceptibility, and hence of the solvent spectral density, which is important in simulating chromophore optical dephasing and solvation in the same medium.[9] Specifically, the high-frequency response ($50-1000\ cm^{-1}$) is important in simulating photon echo responses,[41] whereas the low-frequency region is also important in simulating spectral diffusion and solvation.[21,42] Clearly these responses are also of importance in affecting chemical reaction dynamics,[43] and RS allows for their accurate and well-resolved characterization.

Finally, RS provides the aforementioned advantages over LIA detection in one fourth of the acquisition time and without modulation of the laser fluence directed toward the sample. In addition to the obvious advantage of simply reducing the acquisition time, faster data acquisition makes RS suitable and favorable for the study of weakly absorbing samples or in systems in which only small-amplitude nonlinear polarizations can be induced by the laser pulses.

D. Jitter

The origin of the scan-to-scan jitter noted above is likely due to several sources, some of which are unique to the RS equipment whereas others are due to equipment common to both RS and LIA methods. Those factors that are common to both methods will introduce jitter into LIA measurements as well. However, for the LIA method there is no simple way to differentiate between scan jitter and other fluctuations of the signal. Consequently it is difficult to minimize these effects because one cannot clearly identify or analyze them. Nevertheless, thermal fluctuations in the lab environment seem to be the most significant common cause of jitter for the RS and LIA methods. The consequence of thermal fluctuations is that mirror mounts and stages move slightly as they change temperature. Motions as small as micrometers or less would introduce a measurable jitter into the signal, as light travels 1 μm in 3.33 fs. We tested the significance of thermal fluctuations by intentionally heating and cooling the laboratory while measuring the peak position of the autocorrelation response. Thermal drifts were found to induce significant and reproducible shifts of the autocorrelation's peak data channel. This problem is minimized in our laboratory by tight ($\sim$1 °C) temperature regulation. However, this still may be a contributing factor in the overall scan jitter.

With regard to the equipment specific to the RS method, there seem to be two sources of jitter. First, nonuniform motions, such as bending and shaking, of the velocity transducer or the corner-cube mount will introduce jitter. The calibration and linearization are based on averaged signals and are also subject to the same jitter present in the pump–probe measurements. These nonuniformities contribute to uncertainty in the calibration and linearization process described above (i.e., yielding a variance about the polynomial mean curve) but are not eliminated. Second, the LVDT signal used as a scope trigger is also a source of signal jitter for two reasons: First, the manufacture's stated stability of the LVDT (0.125% full scale) corresponds to approximately four or five scope channels, whereas the oscilloscope's digitizing resolution for the trigger signal corresponds to less than one channel, i.e., $\sim$4 fs, of jitter per sweep. Second, there is some high-frequency noise present in the LVDT position output signal that affects the time at which the scope is triggered.

E. Improvements

Currently we are in the process of improving the RS system to eliminate the need for signal linearization, to limit further the magnitude of scan-to-scan jitter, and to continue to enhance the already excellent SNR. We are proceeding toward these goals in three important ways.

First, the velocity transducer is being upgraded to a new model (VT-1200, Ranger Scientific) with a custom controller interface. This unit operates with an internal laser interferometer to provide continuous velocity feedback to maintain optimum linearity ($<$100 parts in 10^6) and stability. Additionally, a stable scope trigger derived from the interferometrically measured transducer displacement can be used in place of the external LVDT signal. This unit is expected to make the linearization process unnecessary and will minimize the scan jitter currently arising from the velocity transducer and the LVDT trigger.

A second upgrade currently in progress is the adaptation of a portion of the transient signal to serve as the source for a scope trigger. This improved trigger is based on the principles of a constant-fraction discriminator for immunity to intensity fluctuations on the signal. Triggering the digital scope from the actual transient waveform will cause the recorded waveform to be self-triggered, thereby minimizing or eliminating the jitter.

A third upgrade will increase the SRN and the dynamic range of the RS measurements. This will be accomplished by digitizing the signal from a second detector that monitors the dc level of the probe. This monitor will also record the laser noise that is not discriminated against by RS data acquisition but is eventually averaged out. By matching the dc signal amplitudes of the two detectors, continuous dc subtraction can be carried out for a pump–probe configuration through differential amplification of the detector outputs. Alternatively, both detector signals can be recorded in separate scope channels and subtracted on a scan-by-scan basis. In either case the result will be further noise reduction and increased dynamic range of the oscilloscope by the elimination of a large dc offset. Furthermore, for experiments performed in an optical scattering geometry where there is no large dc probe background this subtraction will not be necessary. In any case, compensation for laser intensity fluctuations can yield improvements in SNR and dynamic range.[20,27]

5. SUMMARY AND FUTURE APPLICATIONS

We have presented a new apparatus, based on commercially available equipment, for RS data acquisition in nonlinear spectroscopic experiments. Methods to account for nonequal point spacing and small scan nonlinearities were discussed. The results of OHD-OKE measurements in CCl_4 and mesitylene showed that RS data acquisition obtained 10-fold SNR improvements for six-times-longer scan ranges with five times as many data points in one fourth of the time required in a LIA detection scheme. The spectroscopic quality of the data is considerably enhanced as well; much more accurate line-shape analysis is possible with reduced baseline distortions from slow experimental drifts. Several improvements that are being implemented on the RS apparatus were discussed. These should significantly reduce the present nonlinearity 10-fold to the few-femtosecond level over tens-of-picoseconds scans. Furthermore, probe beam modulations of 10^{-6} versus dc level should be detectable.

The apparatus is currently being used for pump–probe spectroscopic measurements on weakly absorbing samples including dissociative and charge-transfer compounds. Experiments performed in a transient grating geometry, including resonant photon echo measurements[9] and nonresonant scattering studies,[34] are being modified to incorporate this RS acquisition capability. Our efforts toward developing new time-resolved scanned probe microscopies will also benefit from this approach.[44] Obviously, many other spectroscopies will benefit from the application of this reliable and commercially available RS data-acquisition scheme.

APPENDIX A. JONES MATRIX ANALYSIS OF PROBE FIELD AND LOCAL OSCILLATOR FIELD POLARIZATIONS IN OKE EXPERIMENTS

An OKE measurement probes the third-order polarizability tensor, χ_{1212}.[34,35] The first and second electric field interactions are with the horizontal polarization and the vertical polarization components of the pump field, respectively. The third interaction is with the horizontal polarization component of probe field, which has a dominant projection on the horizontal axis for all small rotations of the optical components. The fourth tensor component is the vertically polarized signal field, which is generated with the same phase as the horizontal component of the probe field. Pump-induced transient dichroism and birefringence can be measured by OHD with a local oscillator field that is in phase (dichroism) or $\pi/2$ out of phase, i.e., in quadrature (birefringence) with respect to the signal field and hence to the horizontal component of the probe field. Thus a comparison of the relative phases of the horizontal polarization component of the probe field and the vertical polarization component of the local oscillator can be used to identify the type of OHD signal that can be measured. This comparison of relative phases can be made through a Jones matrix analysis as follows[45]:

General form of Jones matrix analysis with an incident probe field initially polarized horizontally:

$$
\begin{aligned}
E_{\text{probe}} &= [\text{quarter-wave plate}][\text{input polarizer}][\text{incident probe field}] \\
&= \begin{bmatrix} \exp\left(\frac{i\pi}{4}\right)\cos^2\rho + \exp\left(-\frac{i\pi}{4}\right)\sin^2\rho & \sqrt{2}\exp\left(\frac{i\pi}{2}\right)\cos\rho\,\sin\rho \\ \sqrt{2}\exp\left(\frac{i\pi}{2}\right)\cos\rho\,\sin\rho & \exp\left(-\frac{i\pi}{4}\right)\cos^2\rho + \exp\left(\frac{i\pi}{4}\right)\sin^2\rho \end{bmatrix} \begin{bmatrix} \cos^2\theta & \cos\theta\,\sin\theta \\ \cos\theta\,\sin\theta & \sin^2\theta \end{bmatrix} \\
&\quad \times \begin{bmatrix} 1 \\ 0 \end{bmatrix}, \\
E_{\text{lo}} &= [\text{analyzer}][\text{quarter-wave plate}][\text{input polarizer}][\text{incident probe field}] \\
&= \begin{bmatrix} \cos^2\phi & \cos\phi\,\sin\phi \\ \cos\phi\,\sin\phi & \sin^2\phi \end{bmatrix} \begin{bmatrix} \exp\left(\frac{i\pi}{4}\right)\cos^2\rho + \exp\left(-\frac{i\pi}{4}\right)\sin^2\rho & \sqrt{2}\exp\left(\frac{i\pi}{2}\right)\cos\rho\,\sin\rho \\ \sqrt{2}\exp\left(\frac{i\pi}{2}\right)\cos\rho\,\sin\rho & \exp\left(-\frac{i\pi}{4}\right)\cos^2\rho + \exp\left(\frac{i\pi}{4}\right)\sin^2\rho \end{bmatrix} \\
&\quad \times \begin{bmatrix} \cos^2\theta & \cos\theta\,\sin\theta \\ \cos\theta\,\sin\theta & \sin^2\theta \end{bmatrix} \begin{bmatrix} 1 \\ 0 \end{bmatrix}.
\end{aligned}
$$

Condition 1: Crossed polarizers; the fast axis of the quarter-wave plate is parallel to input polarizer transmission axis ($\theta = 0$, $\phi = \pi/2$, $\rho = 0$). Result:

$$
E_{\text{probe}} = \begin{bmatrix} \exp\left(\frac{i\pi}{4}\right) \\ 0 \end{bmatrix}, \qquad E_{\text{lo}} = \begin{bmatrix} 0 \\ 0 \end{bmatrix}.
$$

In this configuration no local oscillator is generated, and optical heterodyne detection is not possible.

Condition 2: Analyzer polarizer rotated to an arbitrary angle ($\theta = 0$, ϕ, $\rho = 0$). Result:

$$
E_{\text{probe}} = \begin{bmatrix} \exp\left(\frac{i\pi}{4}\right) \\ 0 \end{bmatrix},
$$

$$
E_{\text{lo}} = \begin{bmatrix} \exp\left(\frac{i\pi}{4}\right)\cos^2\phi \\ \exp\left(\frac{i\pi}{4}\right)\cos\phi\,\sin\phi \end{bmatrix}.
$$

The vertical polarization component of the local oscillator is in phase with respect to the horizontal polarization component of the probe field. The response measured is dichroism.

Condition 3: Input polarizer rotated to an arbitrary angle (θ, $\phi = \pi/2$, $\rho = 0$). Result:

$$E_{\text{probe}} = \begin{bmatrix} \exp\left(\frac{i\pi}{4}\right)\cos^2\theta \\ \exp\left(\frac{-i\pi}{4}\right)\cos\theta\,\sin\theta \end{bmatrix},$$

$$E_{\text{lo}} = \begin{bmatrix} 0 \\ \sqrt{2}\exp\left(\frac{-i\pi}{4}\right)\cos\theta\,\sin\theta \end{bmatrix}.$$

The local oscillator is in quadrature, i.e., $\pi/2$ out of phase, with respect to the horizontal component of the probe field. The response measured is birefringence.

Condition 4a: Crossed polarizers; the fast axis of the quarter-wave plate is rotated to an arbitrary angle ($\theta = 0$, $\phi = \pi/2$, ρ). Result:

$$E_{\text{probe}} = \begin{bmatrix} \frac{\sqrt{2}}{2}\left[\exp(i2\pi) + \exp\left(\frac{i\pi}{2}\right)\right][\cos^2\rho - \sin^2\rho] \\ \sqrt{2}\exp\left(\frac{i\pi}{2}\right)\cos\rho\,\sin\rho \end{bmatrix},$$

$$E_{\text{lo}} = \begin{bmatrix} 0 \\ \sqrt{2}\exp\left(\frac{i\pi}{2}\right)\cos\rho\,\sin\rho \end{bmatrix}.$$

The horizontal polarization component of the probe field has components that are both in phase (dichroic) and $\pi/2$ out of phase (birefringent) with those of the local oscillator. The relative amplitude of these components is a function of the rotation angle ρ.

Condition 4b: Crossed polarizers; the fast axis of the quarter-wave plate is rotated to a small angle ($\theta = 0$, $\phi = \pi/2$, $|\rho| < 5°$). Result:

$$E_{\text{probe}} = \begin{bmatrix} \frac{\sqrt{2}}{2}\left[\exp(i2\pi) + \exp\left(\frac{i\pi}{2}\right)\right] \\ \sqrt{2}\exp\left(\frac{i\pi}{2}\right)\rho \end{bmatrix},$$

$$E_{\text{lo}} = \begin{bmatrix} 0 \\ \sqrt{2}\exp\left(\frac{i\pi}{2}\right)\rho \end{bmatrix}.$$

The horizontal polarization component of the probe field has two approximately equal components, one in phase (dichroic) and one $\pi/2$ out of phase (birefringent) with respect to the local oscillator.

Rotation of the quarter-wave plate (Condition 4) was chosen over rotation of the input polarizer (Condition 3) for experimental practicality. Rotation of the wave plate was more easily achieved in our configuration, and rotation of the much thicker polarizer would have been more likely to cause misalignment of the probe beam as a function of rotation angle. Thus, because the OHD-OKE signals reported here require subtracting two waveforms with local oscillators of opposite sign, misalignment would lead to distorted waveforms. Further, this procedure, i.e., a local oscillator produced by rotation of the quarter-wave plate, is valid because for far off-resonant OKE measurements the dichroic response is very small and the OHD signal measured is due to birefringence.[46]

ACKNOWLEDGMENTS

We thank the referees for thoughtful comments and for suggesting a few important references. We acknowledge financial support from the Deutsche Forschungsgemeinschaft, the University of Pennsylvania Materials Research Laboratory (DMR-91-20668), National Science Foundation (NSF) SGER grant CHE-9311337, and a NSF National Young Investigator award. N. Scherer is the recipient of a David and Lucille Packard Foundation fellowship and is an Arnold and Mabel Beckman Young Investigator. P. Vöhringer is a Deutsche Forschungsgemeinschaft postdoctoral fellow.

REFERENCES AND NOTES

1. J. Chesnoy and A. Mokhtari, "Resonant impulsive-stimulated Raman-scattering on Malachite Green," Phys. Rev. A **38,** 3566–3576 (1988).
2. F. W. Wise, M. J. Rosker, G. L. Millhauser, and C. L. Tang, "Application of linear prediction least-squares fitting to time-resolved optical spectroscopy," IEEE J. Quantum Electron. **QE-23,** 1116–1121 (1987).
3. I. A. Walmsley, M. Mitsunaga, and C. L. Tang, "Theory of quantum beats in optical transmission-correlation and pump–probe experiments for a general Raman configuration," Phys. Rev. A **38,** 4681–4689 (1988).
4. N. F. Scherer, L. D. Ziegler, and G. R. Fleming, "Heterodyne-detected time-domain measurement of I_2 predissociation and vibrational dynamics in solution," J. Chem. Phys. **96,** 5544–5547 (1992).
5. J. Y. Bigot, M. Portella, R. W. Schoenlein, C. J. Bardeen, A. Migus, and C. V. Shank, "Non-Markovian dephasing of molecules in solution measured with 3-pulse femtosecond photon-echoes," Phys. Rev. Lett. **66,** 1138–1141 (1991).
6. E. J. Nibbering, D. A. Wiersma, and K. Duppen, "Femtosecond non-Markovian optical dynamics in solution," Phys. Rev. Lett. **66,** 2464–2467 (1991).
7. T. Joo and A. C. Albrecht, "Electronic dephasing studies of molecules in solution at room temperature by femtosecond degenerate four wave mixing," Chem. Phys. **176,** 233–247 (1993).
8. P. J. Cong, Y. J. Yan, H. P. Deul, and J. D. Simon, "Non-Markovian optical dephasing dynamics in room-temperature liquids investigated by femtosecond transient absorption-spectroscopy: theory and experiment," J. Chem. Phys. **100,** 7855–7866 (1994).
9. P. Vöhringer, D. C. Arnett, R. A. Westervelt, M. J. Feldstein, and N. F. Scherer, "Optical dephasing on femtosecond timescales: direct measurement and calculation from solvent spectral densities," J. Chem. Phys. **102,** 4027–4036 (1995).
10. D. A. V. Kliner, J. C. Alfano, and P. F. Barbara, "Photodissociation and vibrational-relaxation of I_2 in ethanol," J. Chem. Phys. **98,** 5375–5389 (1993).
11. U. Banin and S. Ruhman, "Ultrafast photodissociation of I_3—coherent photochemistry in solution," J. Chem. Phys. **98,** 4391–4403 (1993).

12. N. Pugliano, D. K. Patlit, A. Z. Szarka, and R. M. Hochstrasser, "Wave-packet dynamics of the HgI_2 photodissociation reaction in solution," J. Chem. Phys. **99,** 7273–7276 (1993).
13. P. C. Becker, H. L. Fragnito, J. Y. Bigot, C. H. Brito Cruz, and C. V. Shank, "Femtosecond photon-echoes from molecules in solution," Phys. Rev. Lett. **63,** 505–507 (1989).
14. R. L. Fork, B. I. Greene, and C. V. Shank, "Generation of pulses shorter than 0.1 psec by colliding pulse mode locking," Appl. Phys. Lett. **38,** 671–672 (1981).
15. D. E. Spence, P. N. Kean, and W. Sibbett, "60-fsec pulse generation from a self-mode-locked Ti-sapphire laser," Opt. Lett. **16,** 42–44 (1991).
16. M. T. Asaki, C. P. Huang, D. Garvey, J. P. Zhou, H. C. Kapteyn, and M. M. Murnane, "Generation of 11-fs pulses from a self-mode-locked Ti-sapphire laser," Opt. Lett. **18,** 977–979 (1993).
17. F. Krausz, Ch. Spielmann, T. Bradec, E. Wintner, and A. J. Schmidt, "Generation of 33-fs optical pulses from a solid state laser," Opt. Lett. **17,** 204–206 (1992).
18. P. Bado and K. R. Wilson, "Experimental picosecond relaxation dynamics of large molecules," J. Phys. Chem. **88,** 655–657 (1984), and references therein.
19. J. M. Halbout and C. L. Tang, "Femtosecond interferometry for nonlinear optics," Appl. Phys. Lett. **40,** 765–767 (1982).
20. M. J. Rosker, F. W. Wise, and C. L. Tang, "Femtosecond relaxation dynamics of large molecules," Phys. Rev. Lett. **57,** 321–324 (1986).
21. M. D. Levenson and S. S. Kano, *Introduction to Nonlinear Spectroscopy*, revised ed. (Academic, London, 1988), Chap. 3, pp. 79–84; Chap. 4, pp. 155–159.
22. M. Maroncelli, "The dynamics of solvation in polar liquids," J. Mol. Liq. **57,** 1–37 (1993).
23. A. C. Tam, "Photoacoutics: spectroscopy and other applications," in *Ultrasensitive Laser Spectroscopy*, D. S. Kliger, ed. (Academic, New York, 1983), pp. 2–108.
24. W. Demtröder, *Laser Spectroscopy* (Springer-Verlag, New York, 1982), p. 385.
25. M. C. Nuss, K. Keller, G. T. Harvey, M. S. Heutmaker, and P. R. Smith, "Amplitude noise reduction of 50 dB in colliding-pulse mode-locking dye lasers," Opt. Lett. **15,** 1026–1028 (1990).
26. M. Rucker, W. Knoll, and J. P. Rabe, "Surface-plasmon-induced contrast in scanning tunneling microscopy," J. Appl. Phys. **72,** 5027–5031 (1992).
27. J. A. Moon, "Optimization of signal-to-noise ratios in pump-probe spectroscopy," Rev. Sci. Instrum. **64,** 1775–1778 (1993).
28. D. C. Edelstein, R. B. Romney, and M. Scheuermann, "Rapid programmable 300 ps optical delay scanner and signal-averaging system for ultrafast measurements," Rev. Sci. Instrum. **62,** 579–583 (1991), and references therein.
29. J. M. Lanzafame, R. J. D. Miller, A. A. Muenter, and B. A. Parkinson, "Ultrafast charge-transfer dynamics at SnS_2 surfaces," J. Phys. Chem. **96,** 2820–2826 (1992).
30. G. C. Cho, W. Kütt, and H. Kurz, "Subpicosecond time-resolved coherent-phonon oscillations in GaAs," Phys. Rev. Lett. **65,** 764–766 (1990).
31. S. E. Ralph and D. Grischkowsky, "THz spectroscopy and source characterization by optoelectronic interferometry," Appl. Phys. Lett. **60,** 1070–1072 (1992).
32. W. S. Pelouch and L. A. Schlie, "Ultrafast band-edge carrier dynamics in $In_{0.65}Ga_{0.35}As$," Appl. Phys. Lett. **65,** 2323–2325 (1994).
33. We know of only one commercial RS system: ODL-150, Clark-MRX, Inc.
34. P. Vöhringer and N. F. Scherer, "Transient grating optical heterodyne detected impulsive stimulated Raman scattering in simple liquids," J. Phys. Chem. **99,** 2684–2695 (1995).
35. D. McMorrow, W. T. Lotshaw, and G. A. Kenney-Wallace, "Femtosecond optical Kerr studies on the origin of the nonlinear responses in simple liquids," IEEE J. Quantum Electron. **24,** 433–454 (1988).
36. D. S. Alavi, R. S. Hartman, and D. H. Waldeck, "A test of continuum models for dielectric friction—rotational diffusion of phenoxazine dyes in dimethylsulfoxide," J. Chem. Phys. **94,** 4509–4520 (1991).
37. Y. J. Chang and E. W. Castner, Jr., "Fast responses from 'slowly relaxing' liquids: a comparative study of the femtosecond dynamics of triacetin, ethylene glycol, and water," J. Chem. Phys. **99,** 7289–7299 (1993).
38. B. Schrader, *Raman/Infrared Atlas of Organic Components*, 2nd ed. (VCH-Verlag, Weinheim, Germany, 1989), pp. A2-02, F8-01.
39. R. W. Helwarth, "Third-order optical susceptibilities of liquids and solids," Prog. Quantum Electron. **5,** 1–68 (1980).
40. The Tektronics TDS 420 scope used in this work can average as many as 10,000 scans.
41. T. S. Yang, P. Vöhringer, D. C. Arnett, and N. F. Scherer, "Simulation and measurement of 3-pulse photon echoes: modeling with spectral densities," submitted to J. Chem. Phys.
42. P. Vöhringer, D. C. Arnett, T. S. Yang, and N. F. Scherer, "Time-gated photon echo spectroscopy in liquids," Chem. Phys. Lett. **237,** 387–398 (1995).
43. B. J. Schwartz and P. J. Rossky, "Aqueous solvation dynamics with a quantum-mechanical solute: computer-simulation studies of the photoexcited hydrated electron," J. Chem. Phys. **101,** 6902–6916 (1994).
44. M. J. Feldstein and N. F. Scherer, "Femtosecond time-resolved scanning tunneling microscopy," submitted to J. Phys. Chem.
45. W. A. Shurcliff, *Polarized Light: Production and Use* (Harvard U. Press, Cambridge, Mass., 1966), Chaps. 2 and 8, App. 2.
46. L. D. Ziegler, R. Fan, A. E. Desrosiers, and N. F. Scherer, "Femtosecond polarization spectroscopy: a density matrix description," J. Chem. Phys. **100,** 1823–1839 (1994).